https://doi.org/10.15407/ufm.27.01.003

N.I. PAVLYSHCHE [1,*] and A.V. KOROTUN [1,2,]**

[1] Zaporizhzhia Polytechnic National University,
64 Universytetska Str., UA-69011 Zaporizhzhia, Ukraine
[2] G.V. Kurdyumov Institute for Metal Physics of the N.A.S. of Ukraine,
36 Academician Vernadsky Blvd., UA-03142 Kyiv, Ukraine

* pavlishchenazar@gmail.com, ** andko@zp.edu.ua

PLASMONIC PHENOMENA IN METALLIC AND METAL–DIELECTRIC PRISMATIC NANOPARTICLES

The optical and plasmonic properties of the metallic and metal–dielectric nanoprisms based on an equilateral triangle are studied. The equivalent spheroid approach is used to obtain the relations for the frequency dependence of the optical characteristics of the studied nanoparticles. The calculations are performed for the frequency dependences of the diagonal components of the polarizability tensor, electric-field enhancement tensor, spectral figure of merit tensor, quality-factor tensor, as well as the extinction cross-section, and radiation efficiency. The size dependences for the frequencies of the transverse and longitudinal surface plasmonic resonances are obtained, and the corresponding estimates are given. The presence of the significant splitting of the surface-plasmonic resonance is proven, and the corresponding estimates are given. The influence of the thickness of the dielectric layer and the sizes of the prismatic metallic core on the behaviour of the studied optical characteristics of the nanostructure is analysed. The influence of the core and shell materials of the prism on the position of the extinction cross-section maxima is demonstrated. The spectral range, in which the radiation efficiency of the studied nanostructures is close to unity, is determined. The comparison of the diagonal components of the tensor optical characteristics is carried out, and the reason for the predominance of the transverse components of the electric-field enhancement, quality factor, and spectral figure of merit tensors over the corresponding longitudinal components is established. The possibilities of using the considered nanostructures to create surface-plasmonic resonance sensors and high-quality optical nanoresonators are discussed.

Keywords: metallic and metal–dielectric nanoprisms, dielectric tensor, polarizability tensor, equivalent spheroid approach, surface-plasmonic resonance, field-enhancement tensors, quality factor and spectral figure of merit, extinction cross-section.

Citation: N.I. Pavlyshche and A.V. Korotun, Plasmonic Phenomena in Metallic and Metal–Dielectric Prismatic Nanoparticles, *Progress in Physics of Metals*, **27**, No. 1: 3–24 (2026)

1. Introduction

The localised surface plasmons are the collective oscillations of electrons that can be excited when incident light interacts with the metallic nanoparticles [1–7]. Under certain conditions, such electron oscillations in the nanoparticle coincide with the frequency of incident light and excite the localised surface-plasmonic resonance (SPR). It is known that the wavelength (frequency) of the localised SPR is very sensitive to changes in the environment, such as the fluctuations in the refractive index or the presence of the analytes. The use of this property of SPR has enabled the development of the highly sensitive and versatile plasmonic sensing method, making SPR a valuable tool for various applications, namely: chemical analysis, environmental monitoring, and biomedical diagnostics [8].

The plasmonic properties of the nanoparticles also depend on other factors: the geometric shape, size, and materials of the nanoparticles [1–7, 9]. The nanoparticles of various shapes have been studied theoretically and experimentally: spheres [10], spheroids [3, 5], discs [11, 12], rods [13, 14], shells [15, 16] and cubes [17], which can be synthesised using the 'wet chemistry' methods or the lithographic methods. The non-spherical nanoparticles demonstrate the significant electric field enhancement and the interaction with the surrounding dielectric medium. This is characteristic of the nanoparticles that have high curvature in certain areas (the neighbourhood of the tips of pyramids, cones, prisms, prolate spheroids, and the ends of cylinders and spherocylinders) [14, 18, 19]. In this regard, nanoprisms are attractive objects with several advantages. In addition to the edges for the enhancement of the electromagnetic fields and, as a result, high sensitivity, nanoprisms have clearly defined geometric parameters, such as height and base side, which provide greater flexibility for tuning the plasmonic properties [20]. Equally important is the availability of the high-performance methods for synthesising the uniform prismatic nanostructures with the adjustable geometric parameters [21].

Noble metals such as Au, Ag, and Cu are widely used as plasmonic materials, mainly due to their low thermal losses and the intense interaction with light in the visible and near-infrared spectral ranges [22]. However, the copper nanoparticles have been less studied in terms of their application as the sensing elements in the plasmonic sensors due to their significant imaginary part of the permittivity and relatively rapid oxidation in air [23]. In turn, the peak of the Au nanoparticle SPR is closer to the interband transitions than that of Ag, which makes it less pronounced, and it has a lower Q-factor [24]. For these reasons, this paper investigates the optical properties of silver nanoprisms.

It should be pointed out that triangular nanoprisms have recently attracted considerable interest for use as the sensing elements in plasmonic sensors [25, 26]. Thus, in works [27, 28], it was reported that thin trian-

gular silver nanoprisms in solution are highly sensitive refractive index sensors in the entire visible and near-infrared wavelength range. The work [29] presents the results of modelling the local electric field and sensitivity factors to changes in the refractive index of hollow triangular gold nanoprisms, noting the significant influence of cavity position on the sensitivity. In Ref. [30], the change in the refractive index sensitivity and the spectral figure of merit (FOM) was investigated as a function of the size and composition of triangular nanoprisms made of Ag–Fe and Au–Fe alloys, while [31] determined the optimal ratio between the sides and the spectral excitation range of SPR sensors using dimeric Au nanoplates of triangular, cubic, hexagonal, and circular shapes. In [32], Fano plasmonic resonance in dimers of triangular nanoprisms was theoretically investigated, and the increase in the spectral figure of merit (FOM) to 16.1 was predicted, while [33] investigated plasmon bands in the silver dimer of triangular nanoprisms, which are connected 'face to face'. It was found that the strong dipole interaction bands are more sensitive than the weak quadrupole interaction bands. In Ref. [34], the ultraviolet plasmonic and sensory properties were investigated in the systems with single and dimer semiconductor triangular prisms, and in Ref. [35], the hybrid plasmonic diffraction sensor was developed using the periodically arranged lattice of gold nanoprisms, which allows both local and bulk refractive indices to be measured. In Ref. [36], the octupolar plasmonic nanosensors based on the ordered arrays of triangular gold nanoprisms are proposed for the detection of ultra-low concentrations of rotavirus.

In recent years, particular attention has been paid to the metal–dielectric nanostructures, in which the combination of materials with the contrasting optical properties allows flexible control of the spectral characteristics and the spatial distribution of the localised plasmonic modes [37–43].

Metal–dielectric nanoprisms exhibit a rich set of plasmonic modes that are sensitive to the size, shape, metal layer thickness, and dielectric environment. The presence of the dielectric component not only reduces the optical losses inherent in the metal systems but also expands the possibilities for controlling the interaction of light with the nanostructure. This makes such systems promising for the creation of highly sensitive sensors, nonlinear optical elements, and platforms for controlling the radiation of quantum sources.

It should be pointed out that despite the existence of the studies on the mechanisms of functioning and application of triangular metal and metal–dielectric nanoprisms as the plasmonic sensors, as well as the numerical studies of the optical properties of the metallic nanoparticles in the form of triangular prisms [44–55], there is no theoretical analysis of the above issues, and therefore it is relevant. This paper discusses the peculiarities of the plasmonic phenomena in metallic and metal–dielectric nanoprisms, analyses the mechanisms of the localised plasmonic resonance

formation, and examines the influence of the geometric and material parameters on their optical response.

2. Mathematical Model

2.1. General Relations

Let us assume that the metallic or metal–dielectric nanoparticle in the form of an equilateral triangular prism is located in the medium with the permittivity ϵ_m (Fig. 1), where the side and thickness of the metallic prism are equal to a and b, correspondingly, and for the metal–dielectric prism, and $b + 2t$, where t is the thickness of the dielectric layer.

We are going to describe the optical properties of the prismatic nanoscale objects, which are under the consideration, within the framework of the equivalent oblate spheroid approach [19, 40–43], the essence of which is as follows: instead of the optical properties of metallic and metal–dielectric nanoprisms, the optical properties of their equivalent metallic and metal–dielectric oblate nanospheroids will be investigated. At the same time, the aspect ratios of equivalent spheroids (the effective aspect ratios) are related to the aspect ratios of the prismatic nanoparticles by the relation that follows from the conditions of the equality of the corresponding axial moments of inertia of the prismatic particles and their equivalent oblate spheroids.

Since a two-layer oblate spheroid, which is equivalent to metal–dielectric nanoprism, has axial symmetry, its permittivity is the second-rank diagonal tensor, and the frequency dependences of its diagonal components have the following form [40, 42]

$$\epsilon_{@}^{\perp(\|)} = \epsilon_s \left\{ 1 + \beta_c \frac{\left(\epsilon_c^{\perp(\|)}(\omega) - \epsilon_s\right)}{\epsilon_s + \left(\epsilon_c^{\perp(\|)}(\omega) - \epsilon_s\right)\left(\mathcal{L}_{\perp(\|)}^{(1)} - \beta_c \mathcal{L}_{\perp(\|)}^{(2)}\right)} \right\}, \tag{1}$$

where ϵ_s is the permittivity of the dielectric shell;

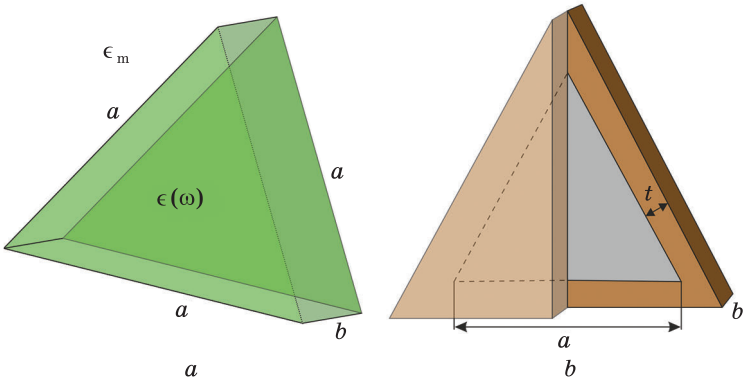

Fig. 1. Geometry of the problem: metallic (*a*) and metal–dielectric (*b*) nanoprisms

$$\beta_{\rm c} = \frac{a^2 b}{\left(a+2t\right)^2 \left(b+2t\right)} \tag{2}$$

is the bulk content of metal in metal–dielectric nanoprism;

$$\mathcal{L}_{\parallel}^{(i)} = \frac{\varrho_{\rm eff}^{(i)2}}{\left(\varrho_{\rm eff}^{(i)2}-1\right)^{3/2}} \left(\sqrt{\varrho_{\rm eff}^{(i)2}-1} - {\rm arctg}\sqrt{\varrho_{\rm eff}^{(i)2}-1}\right), \quad \mathcal{L}_{\perp}^{(i)} = \frac{1}{2}\left(1-\mathcal{L}_{\parallel}^{(i)}\right) \ (i=1,\,2) \tag{3}$$

are the depolarisation factors of the metallic core and the entire equivalent nanoscale oblate spheroid; $\varrho_{\rm eff}^{(1)}$ and $\varrho_{\rm eff}^{(2)}$ are the effective aspect ratios, and the diagonal components of the dielectric tensor of the metallic core and metallic nanoprism are determined by Drude model

$$\epsilon_{\rm c}^{\perp(\parallel)}\left(\omega\right) = \epsilon^{\perp(\parallel)}\left(\omega\right) = \epsilon^{\infty} - \frac{\omega_p^2}{\omega\left(\omega + {\rm i}\,\gamma_{\rm eff}^{\perp(\parallel)}\right)}. \tag{4}$$

In formula (4): ω_p is the plasma frequency, ϵ^{∞} is the contribution of the crystal lattice to the permittivity, and the longitudinal/transverse effective relaxation rates are determined by the additive contributions of three energy loss mechanisms [12, 14]

$$\gamma_{\rm eff}^{\perp(\parallel)} = \gamma_{\rm bulk} + \gamma_{\rm s}^{\perp(\parallel)} + \gamma_{\rm rad}^{\perp(\parallel)}, \tag{5}$$

where the bulk relaxation rate $\gamma_{\rm bulk} = {\rm const}$ for a specific metal, the surface relaxation rate and the radiation damping rate are determined by the relations

$$\gamma_{\rm s}^{\perp(\parallel)} = \mathscr{A}_{\perp(\parallel)} \frac{\upsilon_{\rm F}}{\ell_{\perp(\parallel)}}; \tag{6}$$

$$\gamma_{\rm rad}^{\perp(\parallel)} = \mathscr{B}_{\perp(\parallel)} \frac{\upsilon_{\rm F}}{\ell_{\perp(\parallel)}}. \tag{7}$$

In formulae (6) and (7) $\upsilon_{\rm F}$ is the Fermi electron velocity; $\ell_{\perp} = 2a/\sqrt{5}$, $\ell_{\parallel} = b$ are the effective lengths of the electron free path in the transverse and longitudinal directions, and the size-dependent and frequency dependent functions have the form [42]

$$\mathscr{A}_{\perp(\parallel)} = \frac{9}{16} \frac{\mathcal{L}_{\perp(\parallel)}^{(1)}}{\epsilon_{\rm m} + \mathcal{L}_{\perp(\parallel)}^{(1)}\left(1-\epsilon_{\rm m}\right)} \left(\frac{\omega_p}{\omega}\right)^2 \mathscr{F}_{\perp(\parallel)}\left(\varrho_{\rm eff}^{(1)}\right), \tag{8}$$

$$\mathscr{B}_{\perp(\parallel)} = \frac{9V}{128\pi} \frac{\mathcal{L}_{\perp(\parallel)}^{(1)}}{\sqrt{\epsilon_{\rm m}\left(\epsilon^{\infty} + \dfrac{1-\mathcal{L}_{\perp(\parallel)}^{(1)}}{\mathcal{L}_{\perp(\parallel)}^{(1)}}\epsilon_{\rm m}\right)}} \left(\frac{\omega_p}{c}\right)^3 \left(\frac{\omega_p}{\omega}\right)^2 \mathscr{F}_{\perp(\parallel)}\left(\varrho_{\rm eff}^{(1)}\right), \tag{9}$$

where c is light velocity; $V = \sqrt{3}a^2 b/4$ is the volume of metallic nanoprism

(the core of metal–dielectric nanoprism), and the size factors of equivalent oblate spheroid [42]

$$\mathscr{F}_{\perp}\left(\varrho_{\text{eff}}^{(1)}\right)=\frac{\varrho_{\text{eff}}^{(1)2}}{2\left(\varrho_{\text{eff}}^{(1)2}-1\right)^{3/2}}\left\{\varrho_{\text{eff}}^{(1)}\left(2\varrho_{\text{eff}}^{(1)2}-1\right)\sqrt{\varrho_{\text{eff}}^{(1)2}-1}+\right.$$
$$\left.+\frac{1}{2}\left(4-\frac{3}{\varrho_{\text{eff}}^{(1)2}}\right)\ln\left(\frac{\varrho_{\text{eff}}^{(1)}+\sqrt{\varrho_{\text{eff}}^{(1)2}-1}}{\varrho_{\text{eff}}^{(1)}-\sqrt{\varrho_{\text{eff}}^{(1)2}-1}}\right)\right\}; \tag{10}$$

$$\mathscr{F}_{\parallel}\left(\varrho_{\text{eff}}^{(1)}\right)=\left(\varrho_{\text{eff}}^{(1)2}-1\right)^{-\frac{3}{2}}\left\{\varrho_{\text{eff}}^{(1)}\left(2\varrho_{\text{eff}}^{(1)2}-1\right)\sqrt{\varrho_{\text{eff}}^{(1)2}-1}-\frac{1}{2}\ln\left(\frac{\varrho_{\text{eff}}^{(1)}+\sqrt{\varrho_{\text{eff}}^{(1)2}-1}}{\varrho_{\text{eff}}^{(1)}-\sqrt{\varrho_{\text{eff}}^{(1)2}-1}}\right)\right\}. \tag{11}$$

It should be pointed out that from formula (5), taking into account relations (6)–(9), one can obtain the following expression for the transverse/longitudinal relaxation rates

$$\gamma_{\text{eff}}^{\perp(\parallel)}=\gamma_{\text{bulk}}+\frac{\mathscr{K}_{\perp(\parallel)}}{\omega^2}, \tag{12}$$

where

$$\mathscr{K}_{\perp(\parallel)}=\frac{1}{16}\mathcal{L}_{\perp(\parallel)}^{(1)}\omega_p^2\frac{v_{\text{F}}}{\ell_{\perp(\parallel)}}\mathscr{F}_{\perp(\parallel)}\left(\varrho_{\text{eff}}^{(1)}\right)\times$$
$$\times\left\{\frac{9}{2}\frac{1}{\epsilon_{\text{m}}+\mathcal{L}_{\perp(\parallel)}^{(1)}\left(1-\epsilon_{\text{m}}\right)}+\frac{V}{\pi}\frac{1}{\sqrt{\epsilon_{\text{m}}\left(\epsilon^{\infty}+\dfrac{1-\mathcal{L}_{\perp(\parallel)}^{(1)}}{\mathcal{L}_{\perp(\parallel)}^{(1)}}\epsilon_{\text{m}}\right)}}\left(\frac{\omega_p}{c}\right)^3\right\}. \tag{13}$$

2.2. Effective Aspect Ratios

As noted above, the expression for the effective aspect ratio for a metallic nanoprism can be obtained using the formula

$$\frac{I_x^{\text{prism}}}{I_z^{\text{prism}}}=\frac{I_x^{\text{sph}}}{I_z^{\text{sph}}}. \tag{14}$$

Axial moments of inertia of a triangular equilateral prism

$$I_x^{\text{prism}}=\frac{m_1}{24}\left(a^2+2b^2\right),\ I_z^{\text{prism}}=\frac{m_1a^2}{12}, \tag{15}$$

where m_1 is the mass of the prism, and the axial moments of inertia of the equivalent oblate spheroid

$$I_x^{\text{sph}}=\frac{m_2}{5}\left(a_l^2+b_t^2\right),\ I_z^{\text{sph}}=\frac{2}{5}m_2b_t^2, \tag{16}$$

where m_2 is the mass of spheroid, a_l and b_t are its minor and major semi-axes.

Since for metallic nanoprisms and equivalent metallic spheroids, the aspect ratio and the effective aspect ratio are

$$\varrho = \frac{a}{b}, \quad \varrho_{\text{eff}} = \frac{b_t}{a_l}; \tag{17}$$

then, substituting the expressions (15)–(17) into formula (14), for the effective aspect ratio, we obtain the following

$$\varrho_{\text{eff}} = \frac{\varrho}{\sqrt{2}}. \tag{18}$$

In turn, for metal–dielectric nanoprism and the equivalent metal–dielectric spheroid

$$\varrho_{\text{eff}}^{(i)} = \frac{\varrho^{(i)}}{\sqrt{2}}, \tag{19}$$

where

$$\varrho^{(1)} = \frac{a}{b}, \quad \varrho^{(2)} = \frac{a+2t}{b+2t}. \tag{20}$$

2.3. Polarizability Tensor and the Frequencies of the Surface Plasmonic Resonance

According to the above-described approach of equivalent oblate spheroid, the expressions for the diagonal components of the polarizability tensor of metallic nanoscale prism coincide with the corresponding expressions for the oblate spheroid [19, 42]

$$\alpha_{\perp(\|)} = V \frac{\epsilon^{\perp(\|)}(\omega) - \epsilon_{\text{m}}}{\epsilon_{\text{m}} + \mathcal{L}_{\perp(\|)}\left(\epsilon^{\perp(\|)}(\omega) - \epsilon_{\text{m}}\right)}. \tag{21}$$

The condition for the excitation of the transverse and longitudinal surface plasmonic resonance (SPR) is that the real part of the denominator of the expression (21) is zero

$$\mathbf{Re}\,\epsilon^{\perp(\|)} = -\frac{1-\mathcal{L}_{\perp(\|)}}{\mathcal{L}_{\perp(\|)}}\epsilon_{\text{m}}, \tag{22}$$

from which, in the dissipation-free approximation ($\gamma_{\text{eff}}^{\perp(\|)} \to 0$), we obtain the size dependences for the longitudinal and transverse SPR frequencies

$$\omega_{sp}^{\perp(\|)} = \frac{\omega_p}{\sqrt{\epsilon^{\infty} + \dfrac{1-\mathcal{L}_{\perp(\|)}}{\mathcal{L}_{\perp(\|)}}\epsilon_{\text{m}}}}. \tag{23}$$

In turn, the expressions for the components of the polarizability tensor of a triangular nanoprism, covered with the dielectric layer, have the form similar to the relation (21)

$$\alpha_{@}^{\perp(\parallel)} = V_{@}\frac{\epsilon_{@}^{\perp(\parallel)}(\omega)-\epsilon_{\mathrm{m}}}{\epsilon_{\mathrm{m}}+\mathcal{L}_{\perp(\parallel)}^{(2)}\left(\epsilon_{@}^{\perp(\parallel)}(\omega)-\epsilon_{\mathrm{m}}\right)}, \tag{24}$$

where

$$V_{@} = \frac{\sqrt{3}}{4}\left(a+2t\right)^{2}\left(b+2t\right)$$

is the volume of metal–dielectric nanoprism, and the diagonal components of its dielectric tensor $\epsilon_{@}^{\perp(\parallel)}$ are determined by the relations (1).

By analogy with the expression (22), the condition for the excitation of the transverse/longitudinal SPR in metal–dielectric nanoprism will be as follows

$$\mathbf{Re}\,\epsilon_{@}^{\perp(\parallel)}\left(\omega_{sp}^{@\perp(\parallel)}\right) = -\frac{1-\mathcal{L}_{\perp(\parallel)}^{(2)}}{\mathcal{L}_{\perp(\parallel)}^{(2)}}\epsilon_{\mathrm{m}}, \tag{25}$$

from which the following size dependences of SPR frequencies can be obtained under $\gamma_{\mathrm{eff}}^{\perp(\parallel)} \to 0$

$$\omega_{sp}^{@\perp(\parallel)} = \frac{\omega_{p}}{\sqrt{\epsilon^{\infty}-\epsilon_{\mathrm{s}}+\frac{\epsilon_{\mathrm{s}}}{\beta_{\mathrm{c}}}\dfrac{1+\dfrac{1-\mathcal{L}_{\perp(\parallel)}^{(2)}}{\mathcal{L}_{\perp(\parallel)}^{(2)}}\dfrac{\epsilon_{\mathrm{m}}}{\epsilon_{\mathrm{s}}}}{1+\dfrac{1}{\beta_{\mathrm{c}}}\left(\mathcal{L}_{\perp(\parallel)}^{(1)}-\beta_{\mathrm{c}}\mathcal{L}_{\perp(\parallel)}^{(2)}\right)\left(1+\dfrac{1-\mathcal{L}_{\perp(\parallel)}^{(2)}}{\mathcal{L}_{\perp(\parallel)}^{(2)}}\dfrac{\epsilon_{\mathrm{m}}}{\epsilon_{\mathrm{s}}}\right)}}}}. \tag{26}$$

2.4. Extinction Cross-Section and Radiation Efficiency

As is known, the value, measured in the optical experiments with the nanoparticles of the different shapes and compositions, is the extinction cross-section, the frequency dependences of which for metallic and metal–dielectric nanoprisms are determined as follows [2]

$$C_{\mathrm{ext}} = C_{\mathrm{abs}} + C_{\mathrm{sca}}, \tag{27}$$

$$C_{\mathrm{ext}}^{@} = C_{\mathrm{abs}}^{@} + C_{\mathrm{sca}}^{@}, \tag{28}$$

where the formulas for the absorption and scattering cross-sections of the prismatic nanoparticles, which are under study, have the form

$$C_{\text{abs}} = \frac{\omega}{c}\sqrt{\epsilon_{\text{m}}}\,\text{Im}\left(\frac{2}{3}\alpha_{\perp} + \frac{1}{3}\alpha_{\parallel}\right), \tag{29}$$

$$C_{\text{sca}} = \frac{1}{6\pi}\left(\frac{\omega}{c}\right)^4 \epsilon_{\text{m}}^2\left(\frac{2}{3}\left|\alpha_{\perp}\right|^2 + \frac{1}{3}\left|\alpha_{\parallel}\right|^2\right), \tag{30}$$

$$C_{\text{abs}}^{@} = \frac{\omega}{c}\sqrt{\epsilon_{\text{m}}}\,\text{Im}\left(\frac{2}{3}\alpha_{@}^{\perp} + \frac{1}{3}\alpha_{@}^{\parallel}\right), \tag{31}$$

$$C_{\text{sca}}^{@} = \frac{1}{6\pi}\left(\frac{\omega}{c}\right)^4 \epsilon_{\text{m}}^2\left(\frac{2}{3}\left|\alpha_{@}^{\perp}\right|^2 + \frac{1}{3}\left|\alpha_{@}^{\parallel}\right|^2\right). \tag{32}$$

The radiation efficiency for the nanostructures, which are under consideration, like the extinction cross-section, is determined by the absorption and scattering cross-sections [40]

$$\xi_{\text{rad}} = \left(1 + \frac{C_{\text{sca}}}{C_{\text{abs}}}\right)^{-1}, \tag{33}$$

$$\xi_{\text{rad}}^{@} = \left(1 + \frac{C_{\text{sca}}^{@}}{C_{\text{abs}}^{@}}\right)^{-1}. \tag{34}$$

2.5. Field Enhancement Tensor

Since oblate spheroids, which are equivalent to metallic and metal–dielectric nanoprisms, have axial symmetry, the enhancement of the electric fields in the neighbourhood of the prismatic nanoparticles is represented by the second-rank diagonal tensor, and the frequency dependences of its components will have the following form [19]:
for a metallic prism,

$$\mathscr{F}_{\perp(\parallel)} = \frac{\left(\text{Re}\,\epsilon^{\perp(\parallel)}\right)^2 + \left(\text{Im}\,\epsilon^{\perp(\parallel)}\right)^2}{\left[\mathcal{L}_{\perp(\parallel)}\left(\text{Re}\,\epsilon^{\perp(\parallel)} - \epsilon_{\text{m}}\right) + \epsilon_{\text{m}}\right]^2 + \left[\mathcal{L}_{\perp(\parallel)}\,\text{Im}\,\epsilon^{\perp(\parallel)}\right]^2}; \tag{35}$$

for metal–dielectric prism,

$$\mathscr{F}_{\perp(\parallel)}^{@} = \frac{\left(\text{Re}\,\epsilon_{@}^{\perp(\parallel)}\right)^2 + \left(\text{Im}\,\epsilon_{@}^{\perp(\parallel)}\right)^2}{\left[\mathcal{L}_{\perp(\parallel)}^{(2)}\left(\text{Re}\,\epsilon_{@}^{\perp(\parallel)} - \epsilon_{\text{m}}\right) + \epsilon_{\text{m}}\right]^2 + \left[\mathcal{L}_{\perp(\parallel)}^{(2)}\,\text{Im}\,\epsilon_{@}^{\perp(\parallel)}\right]^2}; \tag{36}$$

here, $\text{Re}\left(\text{Im}\right)\epsilon^{\perp(\parallel)}\left(\epsilon_{@}^{\perp(\parallel)}\right)$ is the real (imaginary) part of the diagonal components of the dielectric tensors of metallic (metal–dielectric) nanoprism.

2.6. Spectral Figure of Merit Tensor

By analogy with other optical characteristics of the prismatic nanoparticles (polarizability tensor, electric field enhancement tensor and dielectric tensors), the spectral figure of merit (FOM) is also the second-rank diagonal tensor [19]

$$\mathrm{FOM}_{ij} = \begin{pmatrix} \mathrm{FOM}_{\perp} & 0 & 0 \\ 0 & \mathrm{FOM}_{\perp} & 0 \\ 0 & 0 & \mathrm{FOM}_{\parallel} \end{pmatrix}, \tag{37}$$

where for the prismatic nanoparticles, which are under consideration,

$$\mathrm{FOM}_{\perp(\parallel)} = \frac{2\sqrt{\epsilon_{\mathrm{m}}}}{\gamma_{\mathrm{eff}}^{\perp(\parallel)}} \frac{\partial \omega_{sp}^{\perp(\parallel)}}{\partial \epsilon_{\mathrm{m}}}, \tag{38}$$

$$\mathrm{FOM}^{@}_{\perp(\parallel)} = \frac{2\sqrt{\epsilon_{\mathrm{m}}}}{\gamma_{\mathrm{eff}}^{\perp(\parallel)}} \frac{\partial \omega_{sp}^{@\perp(\parallel)}}{\partial \epsilon_{\mathrm{m}}}. \tag{39}$$

Taking into account the relations (23) and (26) we finally have: for a metallic prism,

$$\mathrm{FOM}_{\perp(\parallel)} = \frac{\sqrt{\epsilon_{\mathrm{m}}}}{\gamma_{\mathrm{eff}}^{\perp(\parallel)}} \frac{\left(1 - \mathcal{L}_{\perp(\parallel)}\right)\omega_p}{\mathcal{L}_{\perp(\parallel)}\left(\epsilon^{\infty} + \dfrac{1 - \mathcal{L}_{\perp(\parallel)}}{\mathcal{L}_{\perp(\parallel)}}\epsilon_{\mathrm{m}}\right)}; \tag{40}$$

for metal–dielectric prism,

$$\mathrm{FOM}^{@}_{\perp(\parallel)} = \frac{\omega_p\sqrt{\epsilon_{\mathrm{m}}}}{\beta_{\mathrm{c}}\gamma_{\mathrm{eff}}^{\perp(\parallel)}} \frac{1 - \mathcal{L}^{(2)}_{\perp(\parallel)}}{\mathcal{L}^{(2)}_{\perp(\parallel)}} \left\{1 + \frac{1}{\beta_{\mathrm{c}}}\left(\mathcal{L}^{(1)}_{\perp(\parallel)} - \beta_{\mathrm{c}}\mathcal{L}^{(2)}_{\perp(\parallel)}\right)\left(1 + \frac{1 - \mathcal{L}^{(2)}_{\perp(\parallel)}}{\mathcal{L}^{(2)}_{\perp(\parallel)}}\frac{\epsilon_{\mathrm{m}}}{\epsilon_{\mathrm{s}}}\right)\right\}^{-2} \times$$

$$\times \left\{\epsilon^{\infty} - \epsilon_{\mathrm{s}} + \frac{\epsilon_{\mathrm{s}}}{\beta_{\mathrm{c}}} \frac{1 + \dfrac{1 - \mathcal{L}^{(2)}_{\perp(\parallel)}}{\mathcal{L}^{(2)}_{\perp(\parallel)}}\dfrac{\epsilon_{\mathrm{m}}}{\epsilon_{\mathrm{s}}}}{1 + \dfrac{1}{\beta_{\mathrm{c}}}\left(\mathcal{L}^{(1)}_{\perp(\parallel)} - \beta_{\mathrm{c}}\mathcal{L}^{(2)}_{\perp(\parallel)}\right)\left(1 + \dfrac{1 - \mathcal{L}^{(2)}_{\perp(\parallel)}}{\mathcal{L}^{(2)}_{\perp(\parallel)}}\dfrac{\epsilon_{\mathrm{m}}}{\epsilon_{\mathrm{s}}}\right)}\right\}^{-3/2}; \tag{41}$$

here, $\gamma_{\mathrm{eff}}^{\perp(\parallel)}$ in formulae (40) and (41) is calculated using formula (12) for the frequencies $\omega = \omega_{\mathrm{sp}}^{\perp(\parallel)}$ and $\omega = \omega_{\mathrm{sp}}^{@\perp(\parallel)}$, respectively.

2.7. Quality Factor Tensor

From the point of view of using metallic (metal–dielectric) nanoparticles as the optical resonators, the important characteristic is their quality factor (*Q*-factor), since the higher the quality factor, the lower the attenuation in the resonator.

By analogy with other optical characteristics already discussed above, the *Q*-factor is also the second-rank diagonal tensor

$$Q_{ij} = \begin{pmatrix} Q_{\perp} & 0 & 0 \\ 0 & Q_{\perp} & 0 \\ 0 & 0 & Q_{\parallel} \end{pmatrix}; \tag{42}$$

the size dependences and the frequency dependences of its diagonal components are determined by the relations [56]:
for a metallic prism,

$$Q_{\perp(\parallel)} = \frac{\omega}{2\,\mathrm{Im}\,\epsilon^{\perp(\parallel)}(\omega)} \frac{d}{d\omega}\left[\mathrm{Re}\,\epsilon^{\perp(\parallel)}(\omega)\right]; \tag{43}$$

for metal–dielectric prism,

$$Q^{@}_{\perp(\parallel)} = \frac{\omega}{2\,\mathrm{Im}\,\epsilon^{\perp(\parallel)}_{@}(\omega)} \frac{d}{d\omega}\left[\mathrm{Re}\,\epsilon^{\perp(\parallel)}_{@}(\omega)\right]. \tag{44}$$

The Eq. (45) follows from (43) taking into account Eqs. (4) and (12)

$$Q_{\perp(\parallel)} = \frac{\omega^3\left[1 - \dfrac{2\mathscr{K}_{\perp(\parallel)}}{\omega^4}\left(\gamma_{\mathrm{bulk}} + \dfrac{\mathscr{K}_{\perp(\parallel)}}{\omega^2}\right)\right]}{\left(\gamma_{\mathrm{bulk}} + \dfrac{\mathscr{K}_{\perp(\parallel)}}{\omega^2}\right)\left[\omega^2 + \left(\gamma_{\mathrm{bulk}} + \dfrac{\mathscr{K}_{\perp(\parallel)}}{\omega^2}\right)^2\right]}, \tag{45}$$

and the real and imaginary parts of the diagonal components of the dielectric tensor of metal–dielectric prism have the form

$$\begin{aligned} \mathrm{Re}\,\epsilon^{\perp(\parallel)}_{@} = {} & \epsilon_{\mathrm{s}} + \beta_{\mathrm{c}}\epsilon_{\mathrm{s}}\left\{\epsilon_{\mathrm{s}}\left(\mathrm{Re}\,\epsilon^{\perp(\parallel)}_{\mathrm{c}} - \epsilon_{\mathrm{s}}\right) + \left(\mathcal{L}^{(1)}_{\perp(\parallel)} - \beta_{\mathrm{c}}\mathcal{L}^{(2)}_{\perp(\parallel)}\right)\times\right. \\ & \times\left[\left(\mathrm{Re}\,\epsilon^{\perp(\parallel)}_{\mathrm{c}} - \epsilon_{\mathrm{s}}\right)^2 + \left(\mathrm{Im}\,\epsilon^{\perp(\parallel)}_{\mathrm{c}}\right)^2\right]\Big\}\times \\ & \times\left\{\left[\epsilon_{\mathrm{s}} + \left(\mathcal{L}^{(1)}_{\perp(\parallel)} - \beta_{\mathrm{c}}\mathcal{L}^{(2)}_{\perp(\parallel)}\right)\left(\mathrm{Re}\,\epsilon^{\perp(\parallel)}_{\mathrm{c}} - \epsilon_{\mathrm{s}}\right)\right]^2 + \left[\left(\mathcal{L}^{(1)}_{\perp(\parallel)} - \beta_{\mathrm{c}}\mathcal{L}^{(2)}_{\perp(\parallel)}\right)\mathrm{Im}\,\epsilon^{\perp(\parallel)}_{\mathrm{c}}\right]^2\right\}^{-1}; \end{aligned} \tag{46}$$

$$\begin{aligned} \mathrm{Im}\,\epsilon^{\perp(\parallel)}_{@} = {} & \epsilon^2_{\mathrm{s}}\,\mathrm{Im}\,\epsilon^{\perp(\parallel)}_{\mathrm{c}}\left\{\left[\epsilon_{\mathrm{s}} + \left(\mathcal{L}^{(1)}_{\perp(\parallel)} - \beta_{\mathrm{c}}\mathcal{L}^{(2)}_{\perp(\parallel)}\right)\left(\mathrm{Re}\,\epsilon^{\perp(\parallel)}_{\mathrm{c}} - \epsilon_{\mathrm{s}}\right)\right]^2 + \right. \\ & \left. + \left[\left(\mathcal{L}^{(1)}_{\perp(\parallel)} - \beta_{\mathrm{c}}\mathcal{L}^{(2)}_{\perp(\parallel)}\right)\mathrm{Im}\,\epsilon^{\perp(\parallel)}_{\mathrm{c}}\right]^2\right\}^{-1}. \end{aligned} \tag{47}$$

Hereafter, Eqs. (21), (23), (24), (26)–(28), (33)–(36), (40), (41), (44), and (45) will be used to obtain the numerical results, taking into account the expressions (2)–(13), (17)–(20), (29)–(32), (46), and (47).

3. Results of Calculations and Discussion

The optical characteristics were calculated for metallic and metal–dielectric nanoparticles in the shape of a triangular prism. The parameters required for the calculations are given in Tables 1 and 2, respectively.

The frequency dependences of the imaginary parts of the diagonal components of the polarizability tensor are given in Fig. 2. Let us note that these curves are qualitatively similar, but $\max\{\alpha_{@}^{\parallel}\}$ shifted to the higher frequencies compared to $\max\{\alpha_{@}^{\perp}\}$. Since these maxima correspond to the frequencies of the longitudinal/transverse surface plasmonic resonances, for the case of the great effective aspect ratio

$$\Delta\omega_{sp}^{@} = \omega_{sp}^{@\parallel} - \omega_{sp}^{@\perp} \cong \omega_p \left(\frac{1}{\sqrt{\epsilon^{\infty}}} - \sqrt{\frac{\pi}{4\epsilon_s \varrho_{\text{eff}}^{(2)}}} \right). \tag{48}$$

The estimates according to Eq. (48) agree with the numerical results shown in Fig. 2 and give $\hbar\Delta\omega_{sp}^{@} \approx 1.5$ eV.

This significant resonance splitting makes it possible to use prismatic nanoparticles in applications where the selectivity is important. In turn, increasing the thickness of the dielectric layer does not affect the position of the resonance maxima and their amplitudes, but only leads to a slight decrease in the width of the maxima. This is due to the sensitivity of the resonance to changes in the refractive index of the surrounding dielectric layer, rather than to its size.

The frequency dependences of the extinction cross-section are shown in Fig. 3. The calculation results $C_{\text{ext}}^{@}(\omega)$ for nanoprisms with the dielectric

Table 1. **Parameters of metals [19]**

Parameter	Metal				
	Pd	Ag	Pt	Au	Cu
ϵ^{∞}	2.52	3.70	4.42	9.84	12.03
$\hbar\omega_p$, eV	9.7	9.17	15.2	9.07	12.6
$\hbar\gamma_{\text{bulk}}$, eV	0.091	0.016	0.069	0.023	0.024

Table 2. **Parameters of dielectrics [40]**

Dielectric	SiO_2	Al_2O_3	ZnO	Ta_2O_5	Nb_2O_5	TiO_2
ϵ_s	2.10	3.10	4.00	4.67	6.15	6.50

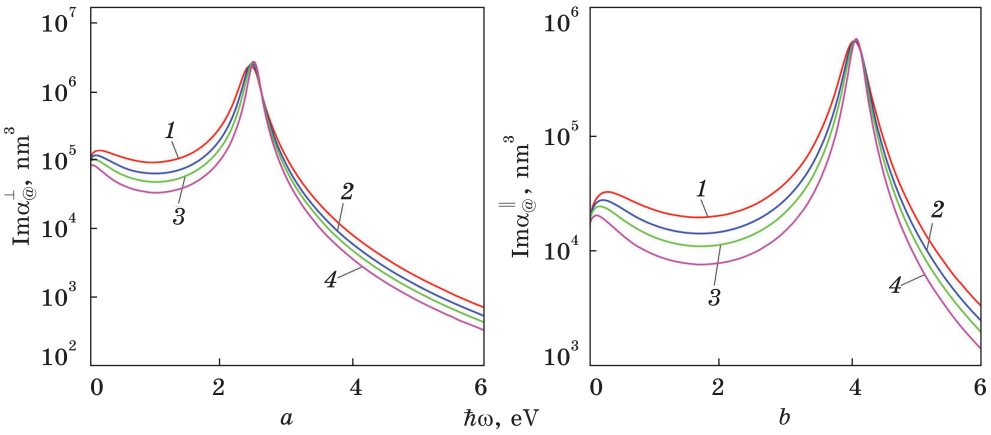

Fig. 2. The frequency dependences of the transverse (*a*) and longitudinal (*b*) components of the polarizability tensor of Au@SiO_2 nanoprisms (a = 80 nm, b = 20 nm) under different thicknesses of the dielectric shell: t = 0 (*1*), t = 2 nm (*2*), t = 4 nm (*3*), and t = 8 nm (*4*)

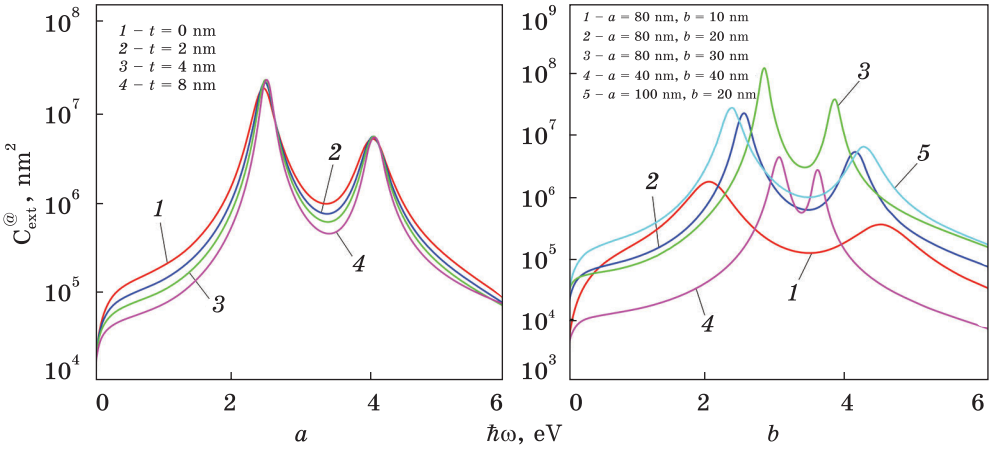

Fig. 3. The frequency dependences of the extinction cross-sections for Au@SiO_2 nanoprisms (a = 80 nm, b = 20 nm) under different thicknesses of the dielectric shell (*a*) and Au@SiO_2 nanoprisms (t = 2 nm) with different sizes (*b*)

coatings of different thicknesses are in good agreement with the corresponding results for $\alpha^{\perp(\parallel)}_{@}(\omega)$, namely, the extinction cross-section curves have two maxima, the positions and the amplitudes of which are not affected by the thickness of the dielectric layer. At the same time, the spectral position of $\max\{C^{@}_{ext}\}$ is strongly influenced by the sizes of the metallic core of metal–dielectric nanoprisms. Thus, an increase in the height of the nanoprism with the constant edge size leads to convergence $\max\{C^{@}_{ext}\}$ and, accordingly, the decrease in the plasmonic resonance splitting (the curves in the sequence 1 → 2 → 3). When the side of the triangular base of the

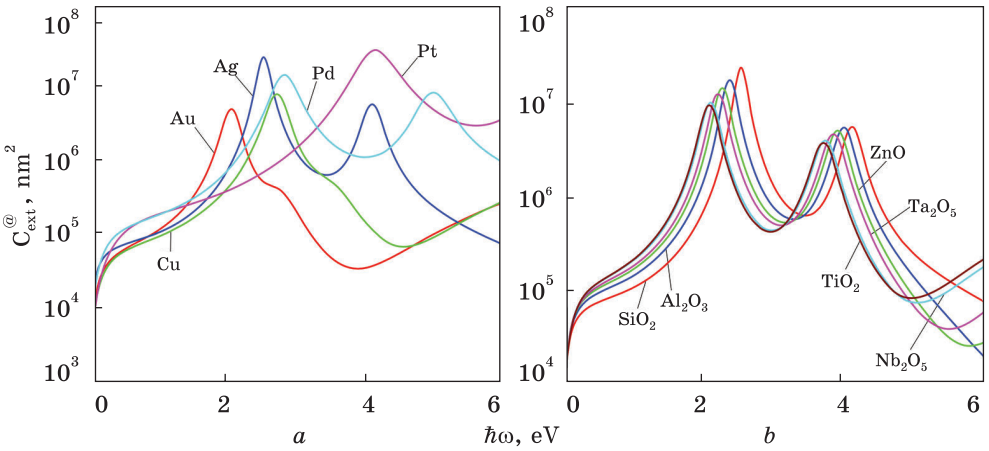

Fig. 4. The frequency dependences of the extinction cross-sections for *Me*@SiO_2 (*a*) and Au@*D* (*b*) nanoprisms at a = 80 nm, b = 20 nm, and t = 2 nm, where *Me* denotes a metal, and *D* designates a dielectric shell

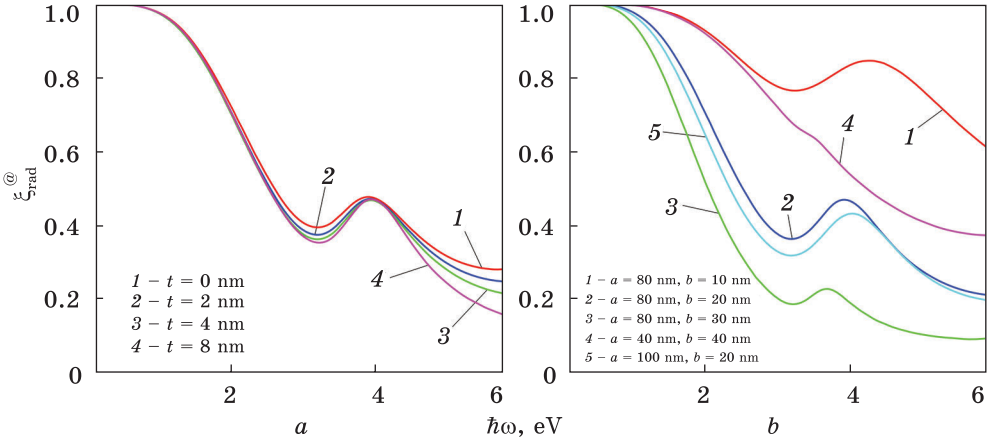

Fig. 5. The frequency dependences of the radiation efficiency of nanoprisms Au@SiO_2 (a = 80 nm, b = 20 nm) under different thicknesses of the dielectric shell (*a*) and nanoprisms Au@SiO_2 (t = 2 nm) with the different geometric sizes (*b*)

prism is increased while the height remains unchanged (the curves in sequence 4 → 2 → 5), there is also a decrease in the plasmonic resonance splitting. The convergence of the extinction cross-section maxima occurs due to the decrease in the splitting of the resonance maximum as the aspect ratio increases.

The information about the influence of the nanoparticle materials (metallic core and dielectric coating) on the extinction cross-sections can be obtained from the curves shown in Fig. 4. It should be pointed out that if the increase in the permittivity of the dielectric coating leads to small

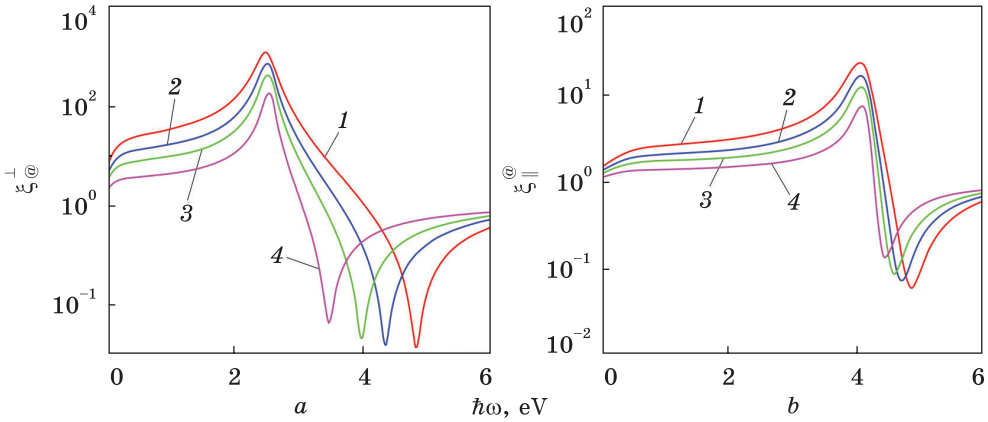

Fig. 6. The frequency dependences of the transverse (*a*) and longitudinal (*b*) components of the electric field enhancement tensor in the neighbourhood of the prismatic nanoparticles Au@SiO_2 (a = 80 nm, b = 20 nm) under different thicknesses of the dielectric shell: t = 0 (*1*), t = 2 nm (*2*), t = 4 nm (*3*), and t = 8 nm (*4*)

'red' shifts in the extinction cross-section maxima, then the corresponding curves for the cores of different metals with the same qualitative character differ significantly in quantitative terms, both in terms of the spectral position and the amplitude. This is due to both the difference in the optical properties of the macroscopic samples of metals, which are under study, and the differences in the structure of their energy bands.

The frequency dependence curves for the radiation efficiency of metallic and metal–dielectric nanoprisms are shown in Fig. 5. It should be pointed out that the influence of the dielectric layer thickness becomes noticeable only in the ultraviolet spectral range, and the radiation*n efficiency will be the maximum ($\xi^{@}_{\text{rad}} \to 1$) in the near-infrared frequency range. In turn, changing the size of the metallic core significantly affects the radiation efficiency in the visible and ultraviolet spectral ranges, with radiation efficiency being highest for nanoprisms with the greatest aspect ratio at any frequency.

The frequency dependences of the diagonal components of the electric field enhancement tensor in the neighbourhood of the prismatic nanoparticles are shown in Fig. 6. The calculated results indicate that $\max\left\{\mathscr{G}_{@}^{\perp(\parallel)}\right\}$ values are achieved at the frequencies of the transverse and longitudinal surface plasmonic resonances, and the amplitudes of the maxima increase with decreasing thickness of the dielectric layer. At the same time, the greatest amplitudes of the transverse and longitudinal field enhancement maxima will occur for a metallic nanoprism. In addition, in the neighbourhood of the surface plasmonic resonance frequencies

$$\frac{\max\left\{\mathscr{G}_{@}^{\perp}\right\}}{\max\left\{\mathscr{G}_{@}^{\parallel}\right\}} \cong 10^2.$$

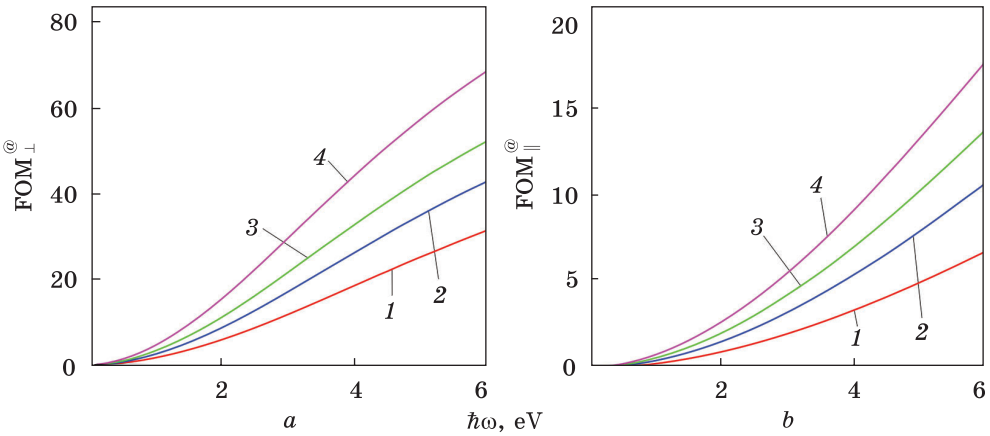

Fig. 7. The same as in the previous figure, but for the spectral figure of merit tensor

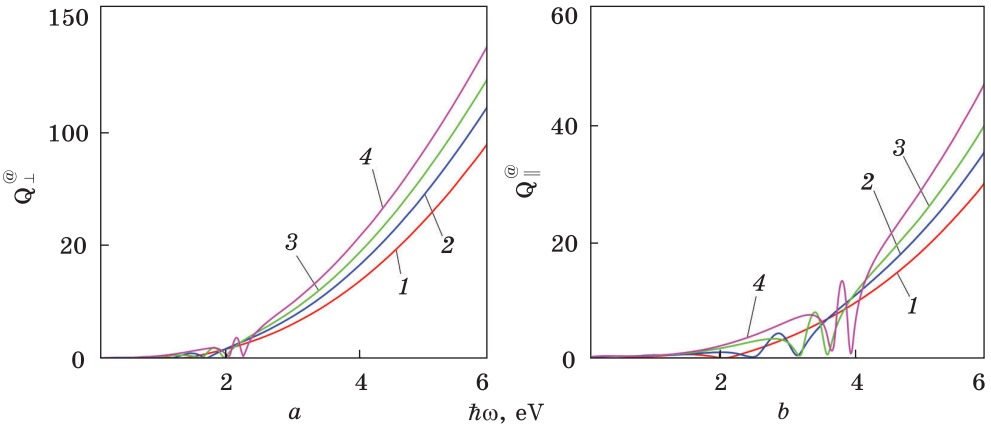

Fig. 8. The same as in the previous two figures, but for diagonal components of the quality factor tensor

Such a significant difference between the transverse and longitudinal components of the field enhancement tensor is due to plasmonic phenomena, which are always more pronounced in the direction associated with the larger size of the nanostructure [19, 40–44].

The frequency-dependent curves of the transverse and longitudinal components of the spectral figure of merit tensor are shown in Fig. 7. As in the case of the field-enhancement tensor, $\mathrm{FOM}^{@}_{\perp} > \mathrm{FOM}^{@}_{\parallel}$. Moreover, if the value $\mathscr{F}^{\perp(\parallel)}_{@}$ increases for each frequency value as the frequency increases and the thickness of the dielectric layer decreases; then, $\mathrm{FOM}^{@}_{\perp(\parallel)}$, conversely, increases as the thickness of the dielectric increases. The behaviour of the components of the spectral figure-of-merit tensor is driven by the reduction in energy losses associated with attenuation of absorption and scattering as the thickness of the dielectric shell increases.

The frequency dependences for the diagonal components of the quality factor tensor are shown in Fig. 8. As in the case of the field-enhancement tensor and the spectral figure of merit tensor, $Q^{@}_{\perp} > Q^{@}_{\parallel}$ at an arbitrary frequency. By analogy with the spectral figure of merit tensor, $Q^{@}_{\perp(\parallel)}(\omega)$ increases with increasing thickness of the dielectric layer. However, in this case, the oscillations $Q^{@}_{\perp(\parallel)}(\omega)$ begin to appear in the infrared, visible, and near-ultraviolet ranges that prevents the use of metal–dielectric nanoprisms with the relatively thick dielectric coatings as the optical resonators.

4. Conclusions

The relations for the frequency dependences of the diagonal components of the polarizability tensor, electric field enhancement tensor, quality factor tensor and spectral figure of merit tensor, as well as the relations for the frequency dependences of the extinction cross-section and radiation efficiency, have been obtained within the framework of the equivalent oblate spheroid approach.

It has been shown that the plasmonic resonance splitting is significant, which makes it possible to use transverse SPR in applications where the absence of the resonance overlap is important.

It has been demonstrated that the thickness of the dielectric coating does not affect the position and amplitude of the imaginary parts of the diagonal components of the polarizability tensor and the extinction cross-section, while the changes in the height and sizes of the edge of the prismatic metallic core lead to the shift in the maxima and the change in their amplitude. At the same time, the convergence of maxima and the decrease in the splitting of the plasmonic resonances occur with the increase in both the height and the length of the side of the triangular base of the nanoprism.

It has been established that the increase in the permittivity of the dielectric shell leads to insignificant ‘red’ shifts of the extinction cross-section maxima, while the change in the core metals leads to the great ‘blue’ shifts of the maxima in the series of metals Au → Ag → Cu → Pd → Pt. This dependence of the spectral position of the extinction cross-section maxima is explained by both the differences in the bulk optical properties of metals and the differences in their energy bands.

It has been shown that the maximum (close to unity) radiation efficiency of the considered nanostructures is achieved in the infrared spectral range, while the thickness of the dielectric layer significantly affects the radiation efficiency in the ultraviolet frequency range. In addition, the radiation efficiency at the same frequency increases with the increase in the aspect ratio.

It has been demonstrated that the diagonal components of the electric field enhancement tensor will be maximal for metallic nanoprisms, and in

the neighbourhood of the surface plasmonic resonance frequencies, the maximum transverse enhancement exceeds the maximum longitudinal enhancement by two orders of magnitude. The difference between the maximum values of the transverse and longitudinal components of the field enhancement tensor is explained by the fact that the transverse dimension of the structures, which are under study, exceeds the longitudinal dimension, and therefore the corresponding plasmonic resonance is more pronounced.

It has been established that, unlike the diagonal components of the field enhancement tensor, the components of the spectral figure of merit tensor increase with increasing thickness of the dielectric layer, which is associated with the weakening of the role of the relaxation processes.

The results of the calculations of the frequency dependences of the diagonal components of the quality factor tensor indicate the possibility of using nanoprisms with a moderate thickness of dielectric coating as the optical nanoresonators, since in this case the quality factor values are greater than for nanoprisms with the thin dielectric layer, and there are no oscillations of the quality factor, which are characteristic of the particles with the thick dielectric shell.

Authors' Contributions. The problem statement belongs to the second author, A.V.K. The review and the analysis of the literature have been carried out by the first author, N.I.P. The analytical approach is developed by both authors. The numerical modelling was performed by N.I.P. The second author, A.V.K., supervised the project, developed the main ideas, verified the analytical approaches, and provided critical comments. Both authors participated in the discussion of the calculation results and the formulation of conclusions. All authors approved the final version of the manuscript.

REFERENCES

1. C.F. Bohren and D.R. Huffman, *Absorption and Scattering of Light by Small Particles* (New York: Wiley-VCH: 1998), p. 545; https://doi.org/10.1002/9783527618156
2. S.A. Maier, *Plasmonics: Fundamentals and Applications* (New York: Springer, 2007), p. 224; https://doi.org/10.1007/0-387-37825-1
3. V. Klimov, *Nanoplasmonics* (New York: Jenny Stanford Publishing: 2013) p. 598; https://doi.org/10.1201/b15442
4. H. Xu, *Nanophotonics*: Manipulating Light with Plasmons (Jenny Stanford Publishing, 2017), p. 250; https://doi.org/10.1201/9781315196619
5. A.O. Koval, A.V. Korotun, Yu.A. Kunytskyi, V.A. Tatarenko and I.M. Titov, *Electrodynamics of Plasmon Effects in Nanomaterials* (Kyiv: Naukova Dumka: 2021), p. 344 (in Ukrainian).

6. N.L. Dmitruk and S.Z. Malinich, *Ukr. J. Phys.*, **9**, No. 1: 3 (2014) (in Ukrainian).
7. V. Amendola, R. Pilot, M. Frasconi, O.M. Maragò, and M.A. Iatì, *J. Phys.: Condens. Matter*, **29**, No. 20: 203002 (2017); https://doi.org/10.1088/1361-648X/aa60f3
8. Q. Duan, Y. Liu, S. Chang, H. Chen, and J.-H. Chen, *Sensors*, **21**, No. 16: 5262 (2021); https://doi.org/10.3390/s21165262
9. K.L. Kelly, E. Coronado, L.L. Zhao, and G.C. Schatz, *J. Phys. Chem. B*, **107**, No. 3: 668 (2003); https://doi.org/10.1021/jp026731y
10. N. Malikova, B. Pastoriza-Santos, M. Schierhorn, N.A. Kotov, and L.M. Liz-Marzán, *Langmuir*, **18**, No. 9: 3694 (2002); https://doi.org/10.1021/la025563y
11. I. Zoric, M. Zach, B. Kasemo, and C. Langhammer, *ACS Nano*, **5**, No. 4: 2535 (2011); https://doi.org/10.1021/nn102166t
12. A.V. Korotun and N.I. Pavlishche, Anisotropy of the optical properties of metal nanodisks, *Optics and Spectroscopy*, **130**, No. 4: 269 (2022); https://doi.org/10.1134/S0030400X22040075
13. J. Pérez-Juste, I. Pastoriza-Santos, L.M. Liz-Marzán, and P. Mulvaney, Gold nanorods: synthesis, characterization, and applications, *Coord. Chem. Rev.*, **249**, Nos. 17–18: 1870 (2005); https://doi.org/10.1016/j.ccr.2005.01.030
14. A.V. Korotun, Ya.V. Karandas, and V.I. Reva, Analytical theory of plasmon effects in rod-like metal nanoparticles. The equivalent-spheroid model, *Ukr. J. Phys.*, **67**, No. 12: 849 (2022); https://doi.org/10.15407/ujpe67.12.849
15. B.L. Sanchez-Gaytan, Z. Qian, S.P. Hastings, M.L. Reca, Z. Fakhraai, and S.-J. Park, *J. Phys. Chem. C*, **116**, No. 18: 10318 (2012); https://doi.org/10.1021/jp300009b
16. A.V. Korotun, A.A. Koval', and I.N. Titov, Optical absorption of a composite based on bilayer metal–dielectric spherical nanoparticles, *J. Appl. Spectrosc.*, **87**: 240 (2020); https://doi.org/10.1007/s10812-020-00991-7
17. S.E. Skrabalak, L. Au, X. Li, and Y. Xia, *Nat. Protoc.*, **2**: 2182 (2007); https://doi.org/10.1038/nprot.2007.326
18. Y. Zhou, H. Li, G. Zhang, D. Wei, L. Zhang, Y. Meng, X. Zheng, X. Sun, and D.Yu, Phys. Chem. *Chem. Phys.*, **22**, No. 35: 19932 (2020); https://doi.org/10.1039/d0cp03470c
19. A.V. Korotun, More on the size effects on the spectral figure of merit and enhancement of the local fields in the neighborhood of biconical and bipyramidal metallic nanoparticles, *Low Temp. Phys.*, **51**, No. 1: 133 (2025); https://doi.org/10.1063/10.0034658
20. M.M. Shahjamali, Y. Zhou, N. Zaraee, C. Ma, G.C. Schatz, and T.W. Odom, *ACS Nano*, **10**, No. 5: 5362 (2016); https://doi.org/10.1021/acsnano.6b01532
21. J.E. Millstone, S.J. Hurst, and G.S. Métraux, *Small*, **5**, No. 6: 646 (2009); https://doi.org/10.1002/smll.200801480
22. P.B. Johnson and R.W. Christy, *Phys. Rev. B*, **6**, No. 12: 4370 (1972); https://doi.org/10.1103/PhysRevB.6.4370
23. K. Sugawa, D. Yamaguchi, N. Tsunenari, K. Uchida, H. Tahara, H. Takeda, K. Tokuda, N. Aoki, K. Yamazaki, N. Takeshima, S. Wakisaka, Y. Kusaka, H. Takekuma,

M. Mitsuishi, J. Otsuki, T. Miyashita, and N. Hayazawa, *ACS Appl. Mater. Interfaces*, **9**, No. 1: 750 (2016);
https://doi.org/10.1021/acsami.6b13147
24. F. Wang and Y.R. Shen, Phys. *Rev. Lett.*, **97**, No. 20: 206806 (2006);
https://doi.org/10.1103/PhysRevLett.97.206806
25. J. Otsuki, K. Sugawa, and S. Jin, *Mater. Adv.*, **2**, No. 1: 32 (2021);
https://doi.org/10.1039/d0ma00644k
26. J.S. Googasian and S.E. Skrabalak, *ACS Phys. Chem. Au*, **3**, No. 3: 252 (2023);
https://doi.org/10.1021/acsphyschemau.2c00064
27. D.E. Charles, D. Aherne, M. Gara, D.M. Ledwith, Y.K. Gun'ko, J.M. Kelly, W.J. Blau, and M.E. Brennan-Fournet, *ACS Nano*, **4**, No. 1: 55 (2009);
https://doi.org/10.1021/nn9016235
28. D.E. Charles, M. Gara, D. Aherne, D.M. Ledwith, Y.K. Gun'ko, J.M. Kelly, W.J. Blau, and M.E. Brennan-Fournet, *Plasmonics*, **6**, No. 2: 351 (2011);
https://doi.org/10.1007/s11468-011-9211-x
29. B. Hazra and M. Chandra, *ACS Sens.*, **1**, No. 5: 536 (2016);
https://doi.org/10.1021/acssensors.5b00314
30. P. Bhatia, S.S. Verma, and M.M. Sinha, *Photonic Sens.*, **9**, No. 3: 246 (2019);
https://doi.org/10.1007/s13320-019-0547-8
31. F. Sun, L. Chen, K. Zhang, and F. Fang, *Plasmonics*, **15**, No. 4: 949 (2020);
https://doi.org/10.1007/s11468-019-01115-4
32. T.-R. Liu, Y. Jiang, C. Qin, S. Jiang, Y. Jiao, X. Zhang, and L. Xiao, *Plasmonics*, **8**, No. 2: 885 (2013);
https://doi.org/10.1007/s11468-013-9486-1
33. A. Azarian and F. Babaei, *J. Appl. Phys.*, **119**, No. 20: 203103 (2016);
https://doi.org/10.1063/1.4952580
34. Z. He, Z. Li, C. Li, W. Xue, and W. Cui, *Opt. Express*, **28**, No. 12: 17595 (2020);
https://doi.org/10.1364/oe.395640
35. K. Akiyoshi, Y.Y. Tanaka, T. Ishida, T. Shimura, and T. Tatsuma, *ACS Appl. Nano Mater.*, **1**, No. 11: 5994 (2018);
https://doi.org/10.1021/acsanm.8b01829
36. M. Rippa, R. Castagna, S. Brandi, G. Fusco, M. Monini, D. Chen, J. Zhou, J. Zyss, and L. Petti, *ACS Appl. Nano Mater.*, **3**, No. 5: 4837 (2020);
https://doi.org/10.1021/acsanm.0c00872
37. A.V. Korotun, A.O. Koval, and V.I. Reva, Optical absorption of composite with bilayer nanoparticles, *J. Phys. Stud.*, **23**, No. 2: 2603 (2019);
https://doi.org/10.30970/jps.23.2603
38. A.V. Korotun, A.A. Koval', and V.I. Reva, Absorption of electromagnetic radiation by oxide-coated spherical metal nanoparticles, *J. Appl. Spectrosc.*, **86**, No. 4: 606 (2019);
https://doi.org/10.1007/s10812-019-00866-6
39. A.V. Korotun, and A.A. Koval', Optical properties of spherical metal nanoparticles coated with an oxide layer, *Opt. Spectrosc.*, **127**, No. 6: 1161 (2019);
https://doi.org/10.1134/S0030400X19120117
40. Ya.V. Karandas, Plasmonic effects in rod-like metal-dielectric nanoparticles, *Condens. Matter Phys.*, 27, No. 2: 23701 (2024);
https://doi.org/10.5488/cmp.27.23701
41. A. Korotun and N. Pavlyshche, Optical absorption of a composite with randomly distributed metallic inclusions of various shapes, *Funct. Mater.*, **29**, No. 4: 567 (2022);
https://doi.org/10.15407/fm29.04.567

42. N.I. Pavlyshche, A.V. Korotun, V.P. Kurbatsky, and V.I. Reva, Plasmon phenomena in metal–dielectric nanodiscs. An equivalent-spheroid approach, *Ukr. J. Phys.*, **70**, No. 4: 263 (2025);
https://doi.org/10.15407/UJPE70.4.263
43. M.S. Maniuk, A.V. Korotun, and V.P. Kurbatsky, Optical response of a chain of oblate metal nanospheroids on a dielectric substrate, *Low Temp. Phys.*, **51**, No. 1: 143 (2025);
https://doi.org/10.1063/10.0034659
44. Y. Xiong, J.M. McLellan, J. Chen, Y. Yin, Z.-Y. Li, and Y. Xia, *J. Am. Chem. Soc.*, **127**, No. 48: 17118 (2005);
https://doi.org/10.1021/ja056498s
45. I. Pastoriza-Santos, A. Sánchez-Iglesias, B. Rodríguez-González, and L.M. Liz-Marzán, *Small*, **5**, No. 4: 440 (2009);
https://doi.org/10.1002/smll.200801088
46. Q. Zhang, J. Ge, T. Pham, J. Goebl, Y. Hu, Z. Lu, and Y. Yin, *Angew. Chem., Int. Ed.*, **48**, No. 19: 3516 (2009);
https://doi.org/10.1002/anie.200900545
47. Y.S. Park and H.K. Chae, *Chem. Mater.*, **22**, No. 23: 6280 (2010);
https://doi.org/10.1021/cm101961g
48. X. Huang, S. Tang, X. Mu, Y. Dai, G. Chen, Z. Zhou, F. Ruan, Z. Yang, and N. Zheng, *Nat. Nanotechnol.*, **6**, 28 (2011);
https://doi.org/10.1038/nnano.2010.235
49. A. Losquin, L.F. Zagonel, V. Myroshnychenko, B. Rodrнguez-González, M. Tencé, L. Scarabelli, J. Förstner, L.M. Liz-Marzán, F.J. Garcнa de Abajo, O. Stéphan, and M. Kociak, *Nano Lett.*, **15**, No. 2: 1229 (2015);
https://doi.org/10.1021/nl5043775
50. F. Qin, X. Cui, Q. Ruan, Y. Lai, J. Wang, H. Ma, and H.-Q. Lin, *Nanoscale*, **8**, No. 40: 17645 (2016);
https://doi.org/10.1039/C6NR06387J
51. Y. Li, Y. Yan, Y. Li, H. Zhang, D. Li, and D. Yang, *CrystEngComm*, **17**, No. 8: 1833 (2015);
https://doi.org/10.1039/C4CE02062F
52. K.W. Smith, J. Yang, T. Hernandez, D.F. Swearer, L. Scarabelli, H. Zhang, H. Zhao, N.A. Moringo, W.-S. Chang, L.M. Liz-Marzán, E. Ringe, P. Nordlander, and S. Link, *J. Phys. Chem. C*, **122**, No. 25: 13259 (2018);
https://doi.org/10.1021/acs.jpcc.7b08428
53. J. Dey, B. Hazra, and M. Chandra, *J. Chem. Phys.*, **151**, No. 11: 114307 (2019);
https://doi.org/10.1063/1.5116528
54. X. Cui, Y. Lai, F. Qin, L. Shao, J. Wang, and H.-Q. Lin, *Nanoscale*, **12**, No. 3: 1975 (2020);
https://doi.org/10.1039/C9NR09976J
55. Y. Zhou, J. Zhu, W. Huang, Z. Wang, K. Li, and W. Huang, *Results in Physics*, **56**, 107314 (2024);
https://doi.org/10.1016/j.rinp.2023.107314
56. A.V. Korotun, H.V. Moroz, and R.Yu. Korolkov, Q-factor of plasmonic resonances and field enhancement in the vicinity of spherical metallic nanoparticles, *Funct. Mater.*, **31**, No. 1: 119 (2024);
https://doi.org/10.15407/fm31.01.119

Received / Final version
13.01.2026 / 04.02.2026

Н.І. Павлище[1], *А.В. Коротун*[1,2]
[1]Національний університет «Запорізька політехніка»,
вул. Університетська, 64, 69011 Запоріжжя, Україна
[2]Інститут металофізики ім. Г.В. Курдюмова НАН України,
бульв. Академіка Вернадського, 36, 03142 Київ, Україна

ПЛАЗМОННІ ЯВИЩА В МЕТАЛІЧНИХ ТА МЕТАЛ-ДІЕЛЕКТРИЧНИХ ПРИЗМАТИЧНИХ НАНОЧАСТИНКАХ

Досліджено оптичні та плазмонні властивості металічних і метал-діелектричних нанопризм, основою яких є рівнобічний трикутник. Для одержання співвідношень для частотних залежностей оптичних характеристик досліджуваних наночастинок використовано підхід еквівалентного сфероїда. Проведено розрахунки частотних залежностей діагональних компонент тензорів поляризовності, підсилення електричних полів, спектральної добротності, добротності, а також перерізу екстинкції та радіаційної ефективності. Одержано розмірні залежності частот поперечного та поздовжнього поверхневих плазмонних резонансів, наведено відповідні оцінки. Доведено наявність значного розщеплення поверхневого плазмонного резонансу, наведено відповідні оцінки. Проаналізовано вплив товщини діелектричного шару та розмірів металевого ядра призматичної форми на поведінку досліджуваних оптичних характеристик наноструктури. Продемонстровано вплив матеріалів ядра й оболонки призми на положення максимумів перерізу екстинкції. Визначено спектральний діапазон, в якому радіаційна ефективність досліджуваних наноструктур близька до одиниці. Проведено порівняння діагональних компонент тензорних оптичних характеристик між собою та встановлено причину домінування поперечних компонент тензорів підсилення електричних полів, добротності та спектральної добротності над відповідними поздовжніми компонентами. Розглянуто можливості застосування проаналізованих наноструктур для створення сенсорів поверхневого плазмонного резонансу та високодобротних оптичних нанорезонаторів.

Ключові слова: металічна та метал-діелектрична нанопризми, діелектричний тензор, тензор поляризовності, підхід еквівалентного сфероїда, поверхневий плазмонний резонанс, тензори посилення полів, добротності та спектральної добротності, переріз екстинкції.